Eur. Phys. J. B **17**, 301–308 (2000)

THE EUROPEAN PHYSICAL JOURNAL B

EDP Sciences

A mechanism for cutting carbon nanotubes with a scanning tunneling microscope

A. Rubio[1,2,a], S.P. Apell[2,3], L.C. Venema[4], and C. Dekker[4]

[1] Departamento de Física Teórica, Universidad de Valladolid, 47011 Valladolid, Spain
[2] Departamento de Física de Materiales, Euskal Herriko Unibertsitatea, Aptdo. 1072, San Sebastian 20080, Basque Country and
Donostia International Physics Center, San Sebastian, Spain
[3] Department of Applied Physics, Chalmers University of Technology and Göteborg University, 41296 Göteborg, Sweden
[4] Department of Applied Sciences and DIMES, Delft University of Technology, Lorentzweg 1, 2628 CJ Delft, The Netherlands

Received 6 April 2000

Abstract. We discuss the local cutting of single-walled carbon nanotubes by a voltage pulse to the tip of a scanning tunneling microscope. The tip voltage ($|V| \geq 3.8$ V) is the key physical quantity in the cutting process. After reviewing several possible physical mechanisms we conclude that the cutting process relies on the weakening of the carbon-carbon bonds through a combination of localized particle-hole excitations induced by inelastically tunneling electrons and elastic deformation due to the electric field between tip and sample. The carbon network releases part of the induced mechanical stress by forming topological defects that act as nucleation centers for the formation of dislocations that dynamically propagate towards bond-breaking.

PACS. 61.16.Ch Scanning probe microscopy: scanning tunneling, atomic force, scanning optical, magnetic force, etc. – 61.48.+c Fullerenes and fullerene-related materials – 62.20.Fe Deformation and plasticity (including yield, ductility, and superplasticity)

1 Introduction

Since the discovery of carbon nanotubes in 1991 [1] a lot of progress has been made in the synthesis as well as in the characterization of the electronic, optical and mechanical properties of these remarkable molecules [2–5]. They are promising structures to use as components in submicrometer-scale devices [6,7] and in nanocomposites [8]. A carbon nanotube can be visualized as a graphite sheet rolled up seamlessly into a cylinder. They have diameters in the range of 0.6–30 nm and are many microns in length. Depending on the synthesis conditions they can appear in multi-walled or single-walled configurations [1,9,10]. The tube symmetry determines not only the electronic (metallic or semiconducting) character [4] but also the plastic/brittle behavior [11,12]. The special geometry makes the nanotubes excellent candidates for mesoscopic quantum wires. Evidence for (1D) quantum confinement was obtained from electronic transport measurements on single-walled nanotubes [13]. The transition from one-dimensional (wire) to zero-dimensional (quantum dot) behavior can be achieved directly by cutting a long nanotube to a shorter length. This has been recently done by Venema *et al.* [14] by applying voltage pulses to the tip of a scanning tunneling microscope (STM) located just above a nanotube. Discrete energy states, consistent with a 1D particle-in-a-box model [15,16], have been measured with STM spectroscopy in such short tubes [15]. The possibility to control the length of nanotubes by the cutting technique is of interest for various applications of carbon nanotubes in nanoscale devices [5,6].

In this paper we discuss a number of possible mechanisms that can explain the experimental observed cutting of tubes by a voltage pulse to the STM tip for single-walled carbon nanotubes. In the following section the experimental data is briefly described. In Section 3, we discuss some relevant physical mechanisms that can result in breaking of tubes and then select one as the most promising mechanism. We analyze the proposed cutting mechanism in Section 4 in more detail and compare the theoretical model to the experimental results. We end the paper with a short discussion and outlook.

2 Experimental results

As found earlier [14] individual carbon nanotubes can be locally cut by applying a voltage pulse to the tip of a scanning tunneling microscope (STM). The carbon nanotubes that were studied were single-walled, synthesized

[a] e-mail: arubio@mileto.fam.cie.uva.es

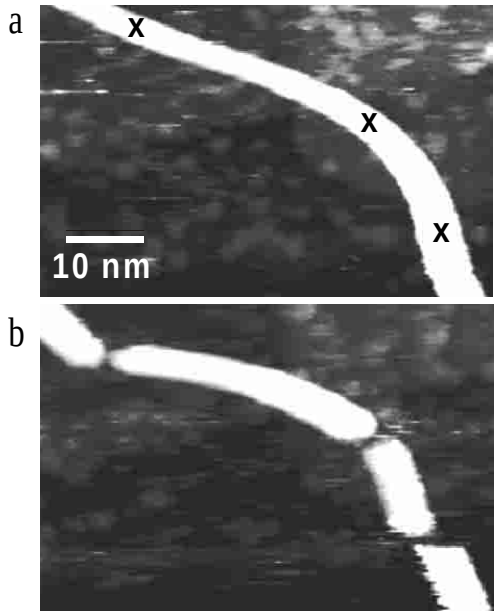

Fig. 1. Room temperature images of a carbon nanotube (a) before and (b) after it was cut at three positions marked with crosses in (a).

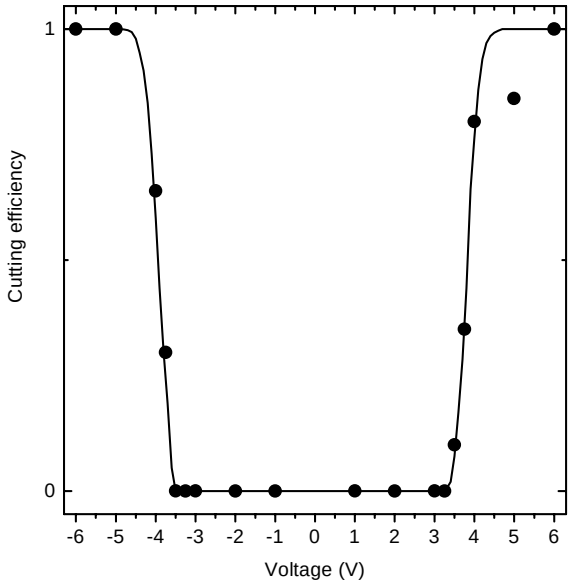

Fig. 2. Cutting efficiency *versus* applied voltage. Efficiency is here defined as the number of successful cuts divided by the total number of applied pulses at that specific voltage. About 150 voltage pulses were applied on various nanotubes. The feedback current was varied between 20 pA and 1 nA; the feedback voltage between 0.1 V and 3 V.

by a laser vaporization technique and consisted mainly of ~ 1.4 nm diameter nanotubes (material from Smalley and coworkers) [9]. Samples were prepared by depositing a dispersion of nanotubes in 1,2-dichloroethane onto single-crystal Au(111) surfaces. The experiments were done both at room temperature and at 4 K.

Nanotubes are cut by the following procedure: During imaging of a nanotube in constant-current mode, scanning is interrupted and the STM tip moves to a selected position on the nanotube. Feedback is then switched off and a voltage pulse between tip and sample is applied for 1 ms. After this pulse, the feedback is switched on again and scanning resumes where imaging was interrupted. The distance between the STM tip and the nanotube during a pulse is determined by the settings for the feedback current and voltage. Figure 1b shows an example of a nanotube that has been cut into various smaller tube pieces as a result of voltage pulses of -3.75 V applied at the positions marked in Figure 1a. Often, tube parts beneath the STM tip are picked up during a pulse. This usually leads to degradation of the tip quality. Cleaning of the tip can then be done by applying voltages on the gold surface, away from the nanotube.

The cutting efficiency as a function of the bias voltage applied during a pulse is shown in Figure 2. This experimental result provides essential input for the theoretical modeling of the cutting mechanism described below. The efficiency at a specific voltage is defined as the number of successful cutting events divided by the total number of applied pulses at that voltage. A large number (about 150) of voltage pulses were applied at room temperature in a range of 1 to 6 V, at positive and negative polarity. The pulses were applied on various nanotubes, both semiconducting and metallic. The separation between nanotube ends created by a cut varies significantly in size, from a few nm to 20 m. Sometimes, the tube ends are displaced after the cut. In particular, Figure 3a shows a strongly bent nanotube on which two voltage pulses were applied near the marked positions. Figure 3b shows that the three tube parts separated by the cuts were moved significantly by the cutting events. Most likely, the nanotube was fixed on the substrate under some strain that was released by the cutting. To study the dependence of cutting efficiency on the distance between the STM tip and the nanotube during a pulse, feedback currents were varied between 20 pA and 1 nA and feedback voltages between 0.1 and 3 V were used. No dependence of cutting efficiency on the tunnel distance was found. Pulses applied with various feedback currents and voltages are therefore included in same graph of Figure 2. The main experimental results are listed below:

- We find a sharp threshold for the voltage of 3.8 ± 0.2 V for cutting nanotubes. This is independent of polarity. Below 3.6 V, nanotubes could almost never be cut. Above 4 V, tubes were almost always cut.
- The cutting efficiency is independent of the feedback tunnel current or voltage. The tunnel resistance has been varied over three orders of magnitude, which changes the tunnel distance significantly. This demonstrates that the determining physical quantity for cutting is the voltage, rather than the electric field.
- The cutting procedure appears to be effective for different types of nanotubes. We observe no dependence on the electronic character (*i.e.* semiconducting or metallic) of a tube.

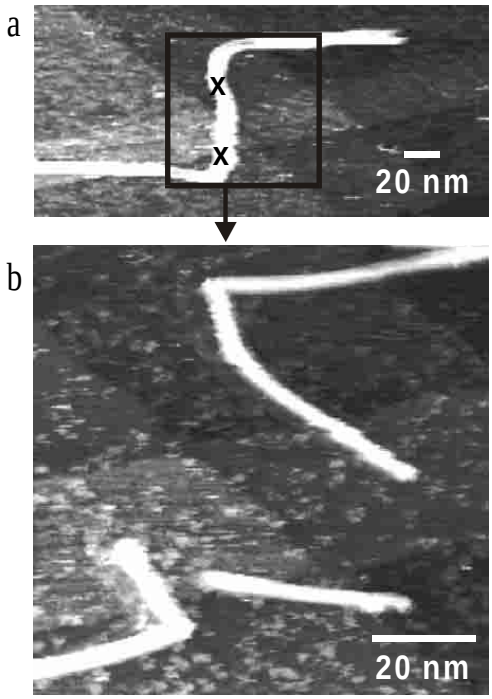

Fig. 3. Room temperature images of a strongly bent nanotube (a) before and (b) after it was cut near the two positions marked with crosses in (a). The three separated tube parts appear to be displaced as a result of the cutting events. Image (b) is an enlargement of the area within the square in (a).

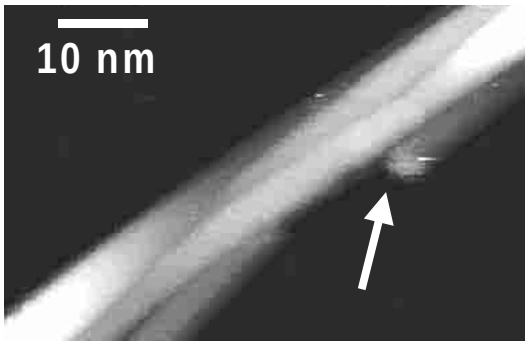

Fig. 4. Room temperature image of a bundle of nanotubes. An individual nanotube within the bundle, indicated by the arrow, could be cut by a voltage pulse.

Table 1. Typical spring constants k [N/m], energy D_0 [eV] needed to break a bond at $T = 0$, and equilibrium distances $R_{\rm eq}$ (Å) for different carbon bonds. In rough terms displacing an atom by 0.1 Å corresponds to an elastic energy change of 5–10 eV.

bond	k (N/m)*	D_0 (eV)*	$R_{\rm eq}$ (Å)*
C-H	460	4.0	1.11
C-C	440	3.4	1.52
C=C	960	7.4	1.34
C≡C	1560	10.0	1.21

* M.F. Ashby, Acta. Metall. **37**, 1273 (1989).

– Nanotubes can be cut at room temperature as well as at 4 K.
– Nanotubes within bundles can be cut as efficiently as isolated single-wall tubes (see for an example Fig. 4).
– Upon decreasing the tunnel distance considerably by increasing the tunnel current beyond 1 nA, nanotubes are moved away laterally by the STM tip during imaging.

3 Physical concepts for the cutting mechanism

In this section we survey a number of possible physical mechanisms for the breaking of nanotubes by a voltage pulse that are interrelated to various degrees [17].

1. *Shear pressure.* Simply crashing the tip into the tube could be a possible cutting mechanism. However, experimentally we find that the tubes are moved laterally when the tip is brought close to the tube. This is related to the large reversible elastic response (flexibility) exhibited by carbon nanotubes [18]. Simulations of C_{60}-molecules impact on carbon nanotubes have shown that even large radial forces produce reversible elastic distortions indicating that crashing the tip onto the tube is not an efficient method to cut [19]. Furthermore, there is no obvious energy scale of 4 eV in the crashing process.

2. *Crack propagation.* This is related to the propagation of voids and cracks already present in as-grown nanotubes under low (tensile) loads. However, there is no evidence, from STM or otherwise, for the presence of local defects or cracks in the SWNT material studied here. This mechanism is hence not considered to be important.

3. *Collective excitations (plasmons).* Plasmons excited by inelastic electron scattering of the tunneling current can decay into electron-hole pairs, phonons or other excitations that induce a polarization or charge separation in the tube. Eventually the release of the plasmon energy leads to a break through local heating and atom evaporation. Due to the particular cylindrical geometry of carbon nanotubes we expect to have a π-plasmon excitation at about 5 eV [20,21]. The decay of the plasmon excitation into atom evaporation is a well-known phenomenon in metallic clusters where the surface-plasmon energy is of the order of the binding energy [22]. In the case of tubes with an internal binding energy greater than ~ 7 eV/atom (as for most carbon solids; see Tab. 1), however, multiple-plasmon excitations need to be active to induce transitions which weaken the carbon bonds. This puts this mechanism behind first-order models, but it can enhance the probability of electronic excitations (see below).

4. *Localized particle-hole excitations.* This mechanism is concerned with the symmetry-allowed interband excitation of localized σ-states to states of π^* character near the Fermi level. These electronic excitations leave localized σ-holes behind which weaken the C-C bonds by creating possible nucleation sites for breaking of the tube. Electrons tunneling inelastically between tip and tube

are the source for these excitations. The probability for this process is favored by the local electric field at the tip-tube interface, which, independent of the metallic or semiconducting behavior, enhances the number of possible bonding/antibonding transitions. The interband excitation involving localized σ-states introduces a natural energy threshold for the cutting process to take place around 3.6 eV. This agrees quite well with the experimental observation of a sharp threshold voltage for cutting of 3.8 eV that is independent of polarity.

5. *Field-induced elastic deformation.* The large electric field from the tip apex causes significant changes in the C-C bond lengths. This introduces a mechanical instability in the tube that triggers the formation of topological defects (for example, double pentagon-heptagon defect pairs, see Fig. 6) [24,25] that dynamically evolve towards breaking of the tube [26]. This effect is enhanced by the stress introduced in the nanotube during the electronic excitation of localized σ-states. The induced stress acts on the tube for the whole 1 ms applied voltage pulse which is long enough for the formation and evolution of the dislocation cores.

The combination of the last two processes is the most likely to constitute the basic mechanism for cutting of nanotubes. The cutting process then is triggered by the inelastic electron excitations involving transitions of localized σ-states at about ~ 3.6 eV. This accounts for the threshold voltage found in the experiments. The C-C bonds are further weakened by the mechanical stress induced by the large electric field between tip and sample. These two processes together induce topological defects and drive the system to mechanical instability. In the next section we present a more detailed analysis of mechanisms 4 and 5 as well as specific molecular dynamics simulations of bond rearrangement and bond-breaking driven by the stress introduced in the nanotube.

4 The cutting mechanism

4.1 Localized electronic excitation

In order to understand the role of electronic excitations in the bond-weakening [27] and cutting process we show in Figure 5 how the density of states of a (10,10) SWNT is modified by an applied electric field in the direction perpendicular to the tube axis. Here the structural relaxation and electronic calculations were done in the framework of the *ab initio* total-energy density-functional pseudopotential theory [28]. We find that the field tends to increase the nanotube's lattice parameter by a few %, nearly independent of the polarity of the applied bias potential. Eventually, as the field strength increases, the structure can reach a state which is not in a stable equilibrium for the carbon atoms any more. The calculations show a slight asymmetry in the response of the carbon nanotube with respect of the applied bias polarity for potentials larger than ± 4 eV [29].

In the calculations shown in Figure 5 the field acts on the whole tube for fixed atomic coordinates. Results are

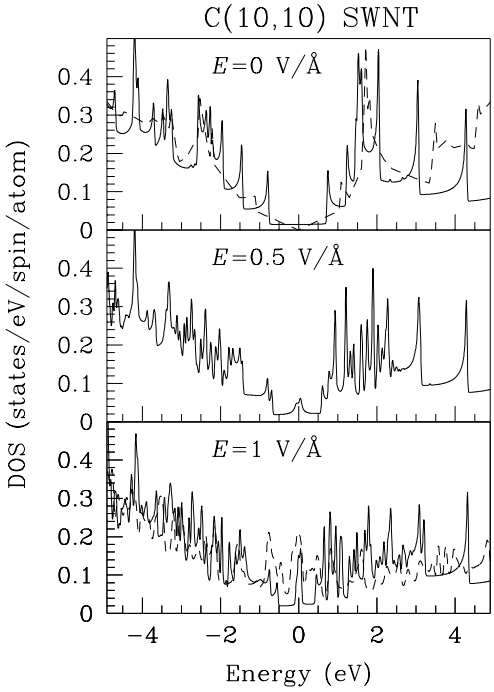

Fig. 5. Density of states of an armchair (10,10) single-wall nanotube for various applied electric fields perpendicular to the tube axis. There is an increase of the density of states at the Fermi level that leads to bond weakening (see text). We also show the results for a field of 4 eV/Å as the dashed line in the bottom panel. For comparison the density of states for a single graphene layer (dash line) is also given in the top panel.

shown corresponding to electric fields accessible in the experimental setup (up to 1 eV/Å). One could also take into account the spatial variation of the applied field related to the tip-size. In that case there are distinct regions: one far from the tip where the electronic properties of the tube are dictated by the isolated tube and the other just beneath the tip where the electronic properties are modified by the applied field. In practice there are field-gradients along the tube that would lead to electrons transport. This effect is not included in our calculations and our aim is to show how the applied voltage modifies locally the density of states DOS of the tube. This local modification can be directly correlated to the weakening and eventual breaking of the carbon bonds.

The DOS for a (10,10) nanotube, which is metallic, is shown in Figure 5. Near the Fermi level, the DOS is finite and constant. At higher energies, sharp peaks can be observed which are the van Hove singularities at the subband onsets [23]. At above/below 3.6 eV from the Fermi level the interband excitations involve states with a predominant σ^*/σ-localized character with a small curvature induced $\sigma - \pi/\sigma^* - \pi^*$ hybridization. The excitations of the σ/σ^* states have been found in nanotubes to lead to a broad spectral feature in the experimental electron-energy loss-spectra close to the π-plasmon excitation [21], similar to the case of $\sigma - \pi^*$ interband transitions in graphite [3] and introduces a natural sharp-voltage threshold as in the experiments. From Figure 5 we see that the applied

field results in the appearance of localized levels which increases the DOS in an energy region close to the Fermi level (this effect is related to the bond-weakening and bond-length increase in carbon nanotubes under an applied voltage discussed above). The increase of density of states near the Fermi level enhances the number of possible transitions that can take place. Semiconducting nanotubes have a DOS comparable to that of metallic nanotubes, but have an energy gap with zero DOS near the Fermi energy. However, the electric field will induce states within the gap, similar to the increase of DOS near the Fermi level for metallic nanotubes. This allows localized particle-hole excitations to take place also for semiconducting nanotubes. Indeed, in the experiments no difference is found in cutting efficiency between semiconducting and metallic nanotubes.

It may appear that any electronic mechanism should be current dependent. However the number of broken bonds is far less than the number of available electrons in the cutting process. The excitations become possible because of the large current available in the STM experiment. The experimental range of currents during the cutting process (more than 50 nA) is such that during the 1 ms pulse more than thousand electrons are involved in inelastic events. This means that we are in a saturated regime where cutting can in principle be achieved independent of the current. This situation can be compared to the situation of cutting Si:H bonds with an STM, where the desorption yield was found to be independent of bias or current once the bias is large enough [30]. The formation of topological defects is a natural way of releasing the excitation energy and naturally triggers the breaking process.

4.2 Field-induced elastic deformation

We study the tip-field induced mechanical stress in the nanotube within a macroscopical approach. An argument for using a macroscopic model is that the specific elastic constants of single wall nanotubes determined from experiments follow quite well the predictions for the macroscopic elasticity theory (in terms of the Young's modulus, Poisson ratio and torsion and bending elastic constants [31]). Although the ultimate description of the fracture mechanics is a complex phenomenon that requires both macroscopic and microscopic descriptions, we thus rely on a continuous model to get a first estimate of the parameters involved in the process. The typical energy of the distortion process is such that it corresponds to bond-breaking energies for carbon compounds (see Tab. 1) or to displacements which fulfill a Lindeman melting criterion [32] of a 10% change in bond distance.

We consider the tube as a thin hollow rod which is clamped to the surface by van der Waals forces. In the cutting process, the tube is distorted by the tip in a region the size of the tip (length-scale L). For a hollow tube (inner radius a and outer radius b) of bending inertia $I = \pi(b^4 - a^4)/4$ and Young's modulus Y, we expect a relative deformation δ for an applied force F of [33]

$$\frac{\delta}{L} \approx \frac{FL^2}{NYI} \tag{1}$$

where N is a number of order 10–100 depending on details of the modeling such as force distribution and boundary conditions. We estimate the force F from the interaction between a sphere of radius R (representing the tip curvature) and a tube of outer radius b (7.5 Å in our situation) to be [34]:

$$F = \frac{\epsilon_0}{d}\sqrt{Rb}(2\pi V)^2 \tag{2}$$

where V is the applied bias voltage and d the tip-tube distance. We see that it depends on the inverse separation. In this equation we have neglected the hollow inner part of the tube that would reduce the force by approximately 20%, but not its dependence on d and V. With $V = 4$ volts, a distance of $d = 10$ Å and $R = 50$ Å (a reasonable value in STM when simulating a tip with a sphere [35]) we find a force of 10 nN [36]. This is independent of the polarity of the bias, as found experimentally. In reference [37] it was observed 1 Å deformation of the graphite surface in an STM configuration for a force of the order of 1 nN. Note however that the relevant elastic constants in their case are related to the weak interlayer bonding in graphite as reflected in the corresponding c_{33} and c_{44} elastic constants (36.5 and 4.5 GPa, respectively). These are much smaller than the c_{11} constant of 1.06 TPa (reflecting the strong intralayer sp^2-like bond) which is relevant in our case [38]. Using now equation (1) and inserting $Y \sim 1$ TPa, we find that for a distortion δ/L higher than the 10% Lindeman criterion, L has at least to be about 5 nm (of course strongly depending on N). Notice that this pull of electro-magnetic origin is happening over the length covered by the tip shape and drops dramatically outside the tip providing a highly "distorted" region.

4.3 Dynamical bond-breaking

Now we address how the electronically and mechanically induced strain can lead to the breakdown of a tube. A plausible mechanism is the Stone-Wales (SW) transformation leading to bond-rotation defects [24]. This comprises of a pair of pentagon-heptagon defects obtained by a simple C-C bond-rotation in the hexagonal network, see Figure 6. These defects are the main source of strain release for tubes under tension [11,12] and determine the overall electronic character of the tube [25]. The pentagon-heptagon defect behaves as a single edge dislocation in the tube circumference. Once nucleated, the pair dislocations can relax further by successive Stone-Wales transformations.

We have performed molecular dynamics simulations of strain-induced defect and plastic/brittle behavior using the tight binding parameterization of reference [39] that reproduces quite well density-functional calculations

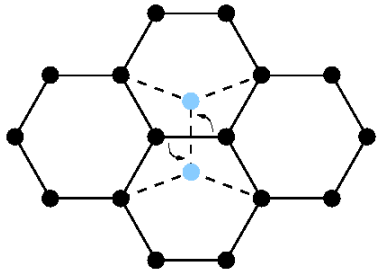

Fig. 6. Schematic description of the strain-induced topological pentagon-heptagon pair defect (Stone-Wales transformation) [24]. The tube axis is in the vertical direction.

within the local-density-approximation. The computed ($T = 0$ K) SW defect formation energy in an armchair nanotube at different applied strains shows that for a tensile strain of about 5% for a (10,10) tube and 12% for a (12,0) tube, the defect geometry is energetically favourable over the perfect tube [40]. The activation barrier for the formation of defects is lowered by the applied tension. Indeed the activation barrier for bond rotation in a (10,10) nanotube is found to reduce from 5.6 eV at zero strain to 3 eV at 10% strain; similar reduction is observed for the barrier for separation of the pentagon-heptagon dislocation cores. The dynamics of these defects are dictated by the tube chirality as well as the applied tension and temperature. In particular at high applied strain and low temperature all tubes are brittle [11]. In the simulations restricted to armchair tubes, we observed that after the nucleation of the first SW-defect, octagonal and higher order rings start to appear as the applied strain is increased. This leads to brittle behavior and shows the important role of the strain induced by the applied voltage. The simulation time scale for the formation and evolution of these defects are of the order of nanoseconds, much shorter than the applied voltage pulse of 1 ms. We thus expect the natural nucleation and evolution of these defects beneath the tip region of the STM, leading to a bond breaking and possible local collapse of the structure.

5 Conclusions and outlook

From the previous discussion we conclude that the applied voltage at the STM tip creates: (i) excitation of localized σ-bonding states, (ii) a change in the density of states around the Fermi level making the tubes more metallic-like and, (iii) an overall distortion of the region beneath the tip, leading to the formation and evolution of strain-induced topological defects. These processes together are responsible for the cutting mechanism with the threshold voltage of $\sim$ 4 V. The proposed mechanism relies only on the applied voltage. It appears that within the experimental values, the tip-tube distance does not change the results.

It would be interesting to attempt the cutting in multi-walled carbon nanotubes also. The cutting will probably not work for these nanotubes since the inner layers are able to accommodate the stress acting on the outer layers. Furthermore we expect the inter-tube van der Waals interaction in multi-walled nanotubes to be strong enough to partially release the concentration of elastic strain so that only atoms of the outer surface will be affected. This is different to the case of nanotubes in bundles, where the cutting process is as effective as for isolated nanotubes (see Fig. 3). In this case the other tubes in the bundle act as a global support similar to the gold substrate for the isolated SWNTs.

It may be interesting to see if the breaking process is accompanied by photon emission to any significant degree to gain further information about the energetic of the possible processes. Photon emission provides a signal that is dependent on the local physical environment beneath the tip with a spatial resolution determined by the size of the local screening charge (collective mode) involved in the photon emission. Typical resolution can be estimated as $\sqrt{Rd} \sim 20$ Å using our length scales introduced above [35,41]. A related topic would be field emission from nano-tubes.

To summarize, we have characterized in detail the possible mechanisms responsible for the breaking up of tubes as found experimentally. Nanotube cutting is a promising technique for the emerging field of nano-manipulation and nanodevices. More studies will have to be made to understand all the interesting physics taking place at this nanoscale level.

This work was supported in part by grants from the Swedish Natural Science Research Council, Iberdrola S.A, JCyL(VA28/99) and the European Community TMR contracts ERB-FMRX-CT98-0198 and ERBFMRX-CT96-0067 (DG12-MIHT). SPA and AR are grateful to the enlightening atmosphere at the University of the Basque Country where most of this work was done. We thank H.L.J. Temminck Tuinstra for help with the experiments and acknowledge discussions with J.W.G. Wildöer, D. Tomanek, P. Bernier and M. Buongiorno-Nardelli. The work at Delft was supported by the Dutch Foundation for Fundamental Research of Matter (FOM).

References

1. S. Iijima, Nature **354**, 56 (1991); P.M. Ajayan, S. Iijima, Nature **361**, 333 (1993).
2. See for example the special issues on *Nanotubes* in Carbon **33** (1996); J. Appl. Phys. A **67** (1998); **68** (1999).
3. M.S. Dresselhaus, G. Dresselhaus, P.C. Eklund, *Science of Fullerenes and Carbon Nanotubes* (Academic Press Inc., San Diego, 1996); M.S. Dresselhaus, G. Dresselhaus, K. Sugihara, I.L. Spain, H.A. Goldberg, *Graphite Fibers and Filaments* (Springer Verlag, 1988).

4. T.W. Ebbesen, *Carbon nanotubes: preparation and properties* (CRC Press, New York, 1997).
5. C. Dekker, Physics Today **52**, 22 (1999).
6. S.J. Tans, A.R.M. Verschueren, C. Dekker, Nature **393**, 49 (1998).
7. J. Liu, A.G. Rinzler, H. Dai, J.H. Hafner, R.K. Bradley, P.J. Boul, A. Lu, T. Iverson, K. Shelimov, C.B. Huffman, F. Rodriguez-Macias, Y. Shon, T.R. Lee, D.T. Colbert, R.E. Smalley, Science **280**, 1253 (1998); P.G. Collins, A. Zettl, H. Bando, A. Thess, R.E. Smalley, Science **278**, 100 (1997).
8. S. Curran, P.M. Ajayan, W. Blau, D.L. Carroll, J. Coleman, A.B. Dalton, A.P. Davey, A. Drudy, B. McCarthy, S. Maier, A. Strevens, Advanced Materials **10**, 1091 (1998); P.M. Ajayan, L.S. Schadler, C. Giannaris, A. Rubio (submitted for publication).
9. A. Thess, R. Lee, P. Nikolaev, H. Dai, P. Petit, J. Robert, C. Xu, Y.H. Lee, S.G. Kim, A.G. Rinzler, D.T. Colbert, G.E. Scuseria, D. Tomanek, J.E. Fisher, R.E. Smalley, Science **273**, 483 (1996).
10. C. Journet, W. Maser, P. Bernier, A. Loiseau, P. Deniard, S. Lefrant, R. Lee, J. Fischer, Nature **388**, 756 (1997).
11. M. Buongiorno-Nardelli, B.I. Yakobson, J. Bernhold, Phys. Rev. Lett. **81**, 4656 (1998); Phys. Rev. B **57**, 4277 (1998).
12. P. Zhang, P.E. Lammert, V.H. Crespi, Phys. Rev. Lett. **81**, 5346 (1998).
13. S.J. Tans, M.H. Devoret, H. Dai, A. Thess, R.E. Smalley, L.J. Geerligs, C. Dekker, Nature **386**, 474 (1997); M. Bockrath, D.H. Cobden, P.L. McEuen, N.G. Chopra, A. Zettl, A. Thess, R.E. Smalley, Science **275**, 1922 (1997).
14. L.C. Venema, J.W.G. Wildöer, H.J.L. Temminck Tuinstra, C. Dekker, A.G. Rinzler, R.E. Smalley, Appl. Phys. Lett. **71**, 2629 (1997).
15. L.C. Venema, J.W.G. Wildöer, S.J. Tans, J.W. Janssen, H.L.J. Temminck Tuinstra, L.P. Kouwenhoven, C. Dekker, Science **283**, 52 (1999).
16. A. Rubio, D. Sanchez-Portal, E. Artacho, P. Ordejón, J.M. Soler, Phys. Rev. Lett. **82**, 3520 (1999).
17. As a starting point for all the possible cutting mechanisms a strong binding between the tube and the substrate is necessary either chemically or through van der Waals forces. Experiments (T. Hertel, R. Martel, P. Avouris, J. Phys. Chem. **102**, 910 (1998); Phys. Rev. B **58**, 13870 (1998)) and first-principle calculations [16] show that tubes have a fairly good binding to the gold substrate. It is typically of the order of 2 meV/atom.
18. S. Iijima, C. Brabec, A. Maiti, J. Bernholc, J. Chem. Phys. **104**, 2089 (1996); M.R. Falvo, G.J. Clary, R.M. Taylor, V. Chi, F.P. Brooks, S. Washburn, R. Superfine, Nature **389**, 582 (1997).
19. A. Lordi, N. Yao, J. Chem. Phys. **109**, 2509 (1998).
20. Note that the imaginary part of the inverse dielectric function for graphite (sheet) has a peak around 6–7 eV, related to a collective plasma excitation [3]. Geometric arguments indicate that for a cylinder this excitation should move down in energy by $\sqrt{2}$.
21. T. Pichler, M. Knupfer, M.S. Golden, J. Fink, A. Rinzler, R.E. Smalley, Phys. Rev. Lett. **80**, 4729 (1998).
22. W.A. de Heer, Rev. Mod. Phys. **65**, 611 (1993); M. Brack, Rev. Mod. Phys. **65**, 677 (1993).
23. A. Rubio, Appl. Phys. A **68**, 275 (1999).
24. A.J. Stone, D.J. Wales, Chem. Phys. Lett. **128**, 501 (1986).
25. V.H. Crespi, M.L. Cohen, A. Rubio, Phys. Rev. Lett. **79**, 2093 (1997).
26. The mechanical deformation might also lead, in some conditions, to jump to contact of tip and sample with potential material transfer between the two. The jump-to-contact voltage can be estimated from the derivative of the elastic and electrostatic forces in equilibrium (O. Hansen, J.T. Ravnkilde, U. Quaade, K. Stokbro, F. Grey, Phys. Rev. Lett. **81**, 5572 (1998)), to be of the order of a few volts depending on the effective tip-sample distance. The jump-to-contact voltage is very sensitive to the equilibrium tunnel gap. This indicates that it is unlikely that we are in this regime here.
27. Removing or adding an electron from/to a tube bond can introduce stresses in the network. So, for instance, the bond length of the C_2-dimer increases from 1.24 to 1.30 Å when taking one electron out, which is a 5% effect. However in more confined structures (*e.g.* benzene) the effect is less relevant as long as the electron is removed from the π-cloud.
28. W.E. Pickett, Comput. Phys. Rep. **9**, 115 (1989); M.C. Payne, M.P. Teter, D.C. Allan, T.A. Arias, J.D. Joannopoulos, Rev. Mod. Phys. **64**, 1045 (1992).
29. This results are in agreement with calculations performed by D. Tomanek, (private communication 1999). Note that the field introduces a quite large mechanical stress in the system. We can estimate from a simple displaced harmonic oscillator model (displacement Δx) the field strength $k\Delta x/e$ necessary for a 10% change in bond distance (Lindemann melting criterion [32]). Using k-values from Table 1 we obtain values of the order of 4 V/Å for the single bond. This corresponds to a change in elastic energy of 6–7 eV. Once this energy is higher than bonding-antibonding transition energies it cannot be accommodated and the bond will tend to break.
30. Ph. Avouris, R.E. Walkup, A.R Rossi, H.C. Akpati, P. Nordlander, T.-C. Shen, G.C. Abeln, J.W. Lyding, Surf. Sci. **363**, 368 (1996).
31. E. Hernández, C. Goze, P. Bernier, A. Rubio, Phys. Rev. Lett. **80**, 4502 (1998); L. Vaccarini, C. Goze, L. Henrard, E. Hernández, P. Bernier, A. Rubio, Carbon (in press).
32. F.A. Lindemann, Z. Physik **11**, 609 (1910).
33. L.D. Landau, E.M. Lifschitz, *Theory of Elasticity*, 2nd edn. (Pergamon, Oxford 1975).
34. B. Derjagin, Kolloid Z. **69**, 155 (1934); L.R. White, J. Colloid Interface Sci. **95**, 286 (1983). To compute the force we use the Derjagin approximation, that was later on elaborated by White. In this approach, the force between two objects is related to the curvatures involved and the interaction energy $E(d)$ per unit area for the corresponding planar situation: $F = 2\pi R_{\text{eff}} E(d)$ where d is the separation between the two solids (average distance between tip and tube in our situation) and R_{eff} expresses the curvatures involved and is given by: $R_{\text{eff}} = R\sqrt{\frac{b}{R+b}} \approx \sqrt{Rb}$. The latter approximation is valid when $R \gg b$, which applies to our case. The interaction energy for two planar surfaces making up a capacitor with a bias voltage V is the classical charging energy: $E(d) = \frac{1}{2}CV^2$. For $C = 4\pi\epsilon_0/d$ (per unit area) we then get the final result for the force given in equation (2).
35. P. Johansson, R. Monreal, P. Apell, Phys. Rev. B **42**, 9210 (1990).

36. It is known from other works (H.F. Budd, J. Vannimenus, Phys. Rev. Lett. **31**, 1218 (1973); Phys. Rev. B **12**, 509 (1975); S. Andersson, B.N.J. Persson, M. Persson, N.D. Lang, Phys. Rev. Lett. **52**, 2073 (1984)) that the classical force used by invoking equation (2) actually reflects an average over the true force acting. There is also a first order response which we should consider since our system is truly microscopic. Within linear response the total force F acting on the ions from an external field E has to average to zero. We checked that this linear term contribution is very small in our particular case.
37. J.M. Soler, A.M. Baro, N. García, H. Rohrer, Phys. Rev. Lett. **57**, 444 (1986).
38. As the shear stress $\mu = Y/(1+\nu)$ is of the same order of magnitude of the Young modulus Y, that is of the order of TPa [31] therefore, we concentrate all the discussion of the cutting on the strain.
39. C.H. Xu, C.Z. Wang, C.T. Chan, K.M. Ho, J. Phys. Condens. Matter **4**, 6047 (1992).
40. Above this critical value the defect density increases rapidly with length [12].
41. Higher resolution and photon intensities can be achieved by taking advantage of the optical-field enhancement at the STM-tip when the tip-surface cavity is illuminated on with a laser. The field enhancement factor is of the order of 1 000 for typical STM-tips and substrates as highly oriented pyrolytic graphite or gold (A.V. Bragas, S.M. Landi, O.E. Martínez, Appl. Phys. Lett. **72**, 2075 (1998)). This new optical microscopy can also be used to study the linear and nonlinear optical response of carbon nanotubes and other nanostructures.